Abstract

We have carried out polarimetric observations to investigate the geometry of the magnetic field in the giant molecular cloud Monoceros R?.. This study is based upon deep R-band CCD polarimetry, covering a total area of 0.5 deg^2 of the giant molecular cloud. The data were calibrated using a new technique that relies on obtaining broad band photometry of stars simultaneously with polarimetric photometry of the Mon R2 fields, thus providing an accurate means of measuring the electric vectors of starlight which is polarized by the foreground dust grains aligned by the magnetic field in the Mon R2 GMC. In this work: (1) we were able to continuously trace magnetic field lines from the largest scales in Mon R2 to the detailed structure of the field in the dense core, as determined from infrared polarimetry, and (2) we have found that the ambient field is apparently modified by a large scale structure in the Mon R2 cloud. Along with gravitational collapse, the cause of the distorted magnetic field is likely to be related to an expanding gas-shell that recent observational results at mm wavelengths now reveal dominates the Mon R2 GMC. The CCD fields are bisected by a dense ridge of gas defining the boundary of the expanding shell. On the eastern (cavity) side of these two fields, stars have low polarizations and, collectively, a high dispersion in the mean angle of polarization; nevertheless, the average angle of polarization is approximately parallel to the ridge. In contrast, along the western side, the vectors suggests continuous magnetic field lines which are approximately parallel to the Galactic plane -- as is true for the global field in the Galactic disk.

Magnetic Field Structure in Monoceros R2

T. H. Jarrett[1]

G. Novak[2,3]

T. Xie[4,5] and P.F. Goldsmith[4,6]

Received _____

[1] NRC Resident Research Associate, Infrared Processing and Analysis Center, Jet Propulsion Lab, California Institute of Technology, Pasadena, CA 91125.

[2] Physics Department, Princeton University.

[3] Currently with the Physics and Astronomy Department, Northwestern University, Evanston Ill. 60208.

[4] Five College Radio Astronomy Observatory, Univ. of Massachusetts, Amherst, MA 01003.

[5] Jet Propulsion laboratory, Pasadena, CA 91109.

[6] National Astronomy and Ionosphere Center, Cornell University, Ithaca, NY 14853.

1. Introduction

For some lime now it has been suspected that magnetic fields play a major role in determining the mass spectrum of stars formed in molecular clouds. Theoretical models of protostellar evolution in a quiescent environment invoke magnetic fields as one form of cloud support and one which has a decisive effect on the minimum stellar mass formed (cf. Shu, Adams and Lizano 1987; Shu *et al.* 1988). The magnetic field also might act as an angular momentum damping mechanism - a vital requirement for gravitational collapse and subsequent star formation (Gil] is, Mestel and Paris 1974; Mouschovias 1978). Empirical evidence of the cent ribution of magnetic fields to the total energetics of molecular clouds comes from analysis of Zeeman splitting of OH absorption and thermal emission lines originating from dense ($n > 10^3$ cm^{-3}) cloud cores (Myers and Goodman 1988; Heiles *et al.* 1991, and references therein). These measurements reveal field strengths as large as one to two orders of magnitude greater than that measured in the diffuse interstellar medium, indicating that magnetic fields are energetically important in dense portions of the lSM.

Measurement of magnetic field strengths in molecular clouds nevertheless remains a formidable task; consequently, efforts are usually focused on determining the *direction* of the magnetic field. We may infer the sky-projected direction of magnetic fields from magnetic alignment of rotating interstellar dust grains. Although slight modifications are apparently in order, the classic Davis & Greenstein (1951) paramagnetic relaxation mechanism is generally assumed to be the correct explanation of the grain alignment phenomenon. Since the grains are anisotropically oriented, starlight shining through cloud will be polarized. "1'bus, measurements of the polarized far-infrared thermal emission from the dust grains and optical and near-infrarc{i polarization by selective extinction of background stars will give the time-averaged direction of the magnetic field (cf. Lee and Draine 1985; Hildebrand 1988). l;ar-infrared polarimetry is useful for studying high opacity regions of molecular clouds, but can only be carried out above the Earth's troposphere. Optical polarimetry has the advantage that it can be accomplished using modest ground-based telescopes, but it has the drawback of being limited to diffuse media and to low opacity regions ($A_v < 5$) of molecular clouds. Near-

infrared polarimetry has been generally limited by the detector technology. With the advent of sensitive large-format CCDs rind near-infrared detectors, optical rind near-infrared polarimetry is now more widely applicable to the overall molecular cloud environment.

Previous radio studies of the molecular gas in Mon R2 (Kutner and Tucker 1975; Loren 1977; Bally and Lada 1983; Maddalena et al. 1986), as wc]] as recent efforts (Myers-Rice and Lada 1991; Xie 1992), and infrared surveys of the embedded population of stars (Beck with *et al.* 1976; Thronson *et al.* 1980; 1 lackwell *et al.* 1982) have revealed this to be a kinematically complex region undergoing vigorous high-mass star formation. Analogous to polarimetric studies of dense molecular clouds (cf. Dyck and Lonsdale 19'/9), there is some evidence that magnetic fields play an important role in relatively lligll-energy environments such as Mon R2. The results of far-infrared polarimetry of Orion A (Novak *et al.* 1989; 1990) suggest that the magnetic field possesses a substantial degree of order and has played a role in the formation of massive stars in this GMC. Sato et al. (1988) claim that some of the flattened structures seen in the ρ Ophiuchi cloud arc consistent with gravitational collapse along the ambient magnetic field. Likewise, optical and infrared polarimetry of the Mon R2 *core* region (Hodapp 1987; Zaritsky et *al.* 1987; Aspin & Walther 1990) reveal a magnetic field geometry consistent with gravitational contraction primarily along the direction of an energetically important magnetic field. The apparent long axis of the Mon R2 core region is perpendicular (o the average magnetic field direction, and the field lines suggest curvature possibly duc to contraction along the direction perpendicular to the field. Furthermore, the magnetic field direction is parallel to the long axis of the high velocity bipolar molecular outflow (cf. Bally and Lada 1983) centered near the cmbcddcd infrared-clus[er. A field direction - outflow axis coincidence has also been observed in other molecular clouds (I lodapp 1984; Strom et *al.* 1986). Theoretical modeling of low-mass star formation tends to favor a scenario in which cloud collapse starts along the magnetic field direction, forming flattened structures (e.g. Shu, Adams and Lizano 1987); however, no consistent empirical evidence have thus far been obtained to verify this (*e.g.* Vrba, Strom and Strom, 1976 and 1988; 1 leyer *et al. 1986;* Goodman *et al.* 1990). A more conclusive association between star formation and

magnetic fields comes from a study by Aitken et al. (1993), which finds that most high-mass protostellar objects possess a magnetic field direction that lies in" the plane of their toroidal disks (i.e., perpendicular to the outflow axis). This result underscores the complexity of protostellar evolution in which the gas undergoes stages of gravitional collapse and mass outflow, all the while influenced by cloud rotation and the ambient magnetic field. In addition to local environmental factors, the star formation may also be influenced by large scale events, such as shock waves from nearby supernova or winds from O stars. The Mon R2 GMC is a good example. To date, the most extensive view of the complex gas structure of the Mon R2 region comes from the mm-wave study of Xie (1992) and Xie, Goldsmith and Patel (1993). They describe the bipolar outflow as consisting of "eggplant-shaped" components partly compressed by what they observe to be a blue-shifted (supersonic) expanding shell or bubble that is propagating through the Mon R2 giant molecular cloud.

In this paper we present CCD R-band polarimetric observations of stars located behind the Mon R2 giant molecular cloud (d - 850 pc; Herbst and Racine, 1976; Loren *1977).* Our goal is to investigate the overall magnetic field geometry in this high-mass star formation region; until recently, it has not been feasible to map magnetic fields throughout an entire GMC. By combining techniques for studying the field in dense regions (infrared polarimetry) with optical CCD polarimetric techniques to measure the magnetic field structure at the largest scales (this study), we may better understand issues related to the ISM and star-formation, as well the role of magnetic fields in GMCs in relation to the Galaxy as a whole (Parker instabilities, spiral density waves, etc.). We present the observations, data and calibrations in the following section, including a brief discussion of the new polarimetric technique used in this study. In a separate paper (Novak and Jarrett 1993) we discuss in greater detail our polarimetric technique. The results of the polarimetry are presented in §3, followed in §4 by a discussion] of the magnetic field structure in Mon R2.

"2. Observations and Data

The polarimetric data collected in this program consist of optical CCD im'ages of fields..l.oward the Mon R2 molecular cloud complex. The observations were carried out over ii period of three nights beginning January 24, 1992, using a Tek 2048 CCD camera mounted (f/7.5) to the Kitt Peak National Observatory 0.9-m telescope. A summary of the physical characteristics of the detector as well as the telescope can bc found in the 1990 manual *operation of the CCD Direct Imaging Camera for the* 0.9 *Meter Telescope Kitt Peak National Observatory,* by II. Schoening et ai..

Four linear polarizing filters, with position angles O0 90°, *45°*, and 135°, were loaded into a rotating filter-wheel assembly. The polarizers arc commercially available photographic filters, with one important modification. A small hole of size 9/16″ was drilled out of the center of each polaroid filter. The effective area of the hole is roughly 12 - 15% of the CCD field. A Cousins R_c broadband filter, held in a fixed position directly in front of the filter-wi~ccl, was employed in tandem with the polaroid fillers and CCD to complete the polarimetric detector system. With this configuration, roughly 85% of the CCD field is subject to an R-band/polaroid filter combination, while the remaining -1596 of the field is screened through the R filter alone.

Three CCD fields were imaged in Mon R2 using the R-band and polaroid filler combination. The field areas were -23' x 23' each, centered at locations (epoch 1950): 1) $\alpha = 6^h$ 05"'21', $\delta =$ -6°22'33", 2) 6" 04^m 36^s, -6°05"29", and 3) 6^h 04"' 46.2^s, -5°39'51". in addition to the polarimetry data, V and 1 images were obtained for the Mon R2 fields to provide color information, while fields which included Landolt flux standard stars (Landolt 1983) and known polarized stars were obtained to provide calibration information. The calibrations are described in the following section.

2.1 Data Reductions

Each raw CCD image was subject to bias and dark current corrections, flat-field division, cleaned of cosmic rays bits and cosmetic anomalies, and corrected for atmospheric extinction. lRAF routines were used for these corrections and the extinction coefficients were checked against mean site

values. The average R-band extinction coefficient was determined to be -O.] 85, which is roughly a factor of two larger than the mean KPNO value averaged over a' ten year period or so (G. Jacoby, private communication). This 'additional' extinction probably resulted from the tiny ice particles in the upper atmosphere that formed from SO_2 gas released from the recent 1991 Mt. Pinatubo eruption. Next, the images were corrected for variations in atmospheric transmission. This correction was determined from stars located in the *center* of the image where the filter hole was aligned with the CCD field; and thus, the intensities were subject to the R-band filter only. in this way we are able to correct for small transmission differences between exposures of the four polarizing filters.

The next step was to perform synthetic aperture photometry for the stars located within the portion of the CCD field subject to the polarizing filters. A series of 4 or 5 exposures were taken for each polaroid orientation, 0°, 90°, 45° and .135°. '['he intensities of each filter were combined into the normalized Stokes parameters, q and u, and averaged to obtain the final estimates of the Stokes parameters, $\bar{q}$ and $\bar{u}$. Here we have followed the conventions of Serkowski (1974). In Novak and Jarrett (1993) we describe in detail the method we used to estimate the uncertainties that apply to $\bar{q}$ and $\bar{u}$. Briefly, our method was to use the standard deviation of the individual measurements of Stokes parameters q and u to determine the uncertainties. However, we modified this procedure somewhat to account for the small number of exposures at each polarization angle. The conversion to the degree, P, and angle, O, of polarization, and their associated uncertainties, follows in the standard Way.

Each star is assigned a V, R, and I magnitude based on the broadband images taken at the end of the observing run. From Landolt standards, we determine the (p-R), (r-l<), (V-R) and (V-1) color transformation coefficients, where r is the raw R-band magnitude, and p is the raw magnitude of the R plus polaroid-filter combination. The photometric accuracy of the color transformations is -1 0%, which is not a major concern since the primary focus of this study is to measure accurate polarimetric fluxes.

2.2 Polarimetry Calibrations

. . in order to determine the instrumental polarization, we observed a number of unpolarized stars . . ." located in the M67 cluster, as well as one highly polarized source in the 1.1641 cloud of Orion. A more complete discussion is given in Novak and Jarrett (1 993).

The old galactic cluster M67 serves as an excellent calibration field owing to its close proximity (750 pc; Eggen and Sandage 1964), abundant population and minimal obscuration (Janes and Smith 1984). The polarizations of these stars have not been independently measured, but are probably <0.3% (see below). We computed the Stokes parameters for bright stars (R <13) located uniformly throughout the CCD field. On average we measure 0.2% as the degree of polarization. "To test the uniformity of the filters/detector combination we divided the CCD field into 8 contiguous zones, each of size - 7.7' x 7.7'. The degree of polarization in each zone is comparable to the ensemble average and there is no indication of a transmission gradient across the field. We conclude that the upper limit to the instrumental polarization is <0.3% (Novak and Jarrett 1993). Although we make no correction for this effect in the measured stokes parameters, we do add 0.3% in quadrature to the estimated stokes uncertainty AI'.

As a further check of our methods and detector capabilities, we observed the highly polarized source VSS 185 (Vrba, Strom and Strom 1988) located toward the L]641 molecular cloud. The measured polarization of VSS185, 7.3 ± 0.7%, is consistent with the published value of VSS, 6.9 ± 0.6%, within the 1σ error limit. The angle of polarization, 70 ± 4°, is within 2σ of the VSS value 61 ± 10. We conclude that the methods used in this study to measure linear polarization of stars provide results that are consistent with those measured using standard techniques.

3. Results

Three 23′ × 23′. CCD held: were observed toward the Mon R2 region. The first field . ," (henceforth, Mon R2 Core) is centered on the dense core of' the Mon R2 molecular cloud, and includes as well the powerful bipolar molecular outflow observed by Loren (197'/) and Bally and Lada (1983). The second field (Men R2 NW) lies roughly 17′ north and 12′ west of the core. The third field (Men R2 NN) lies roughly 42′ north and 8′ wcs(of the core.

In Mon R2 Core wc detected -180 stars with S/N ratios >50:1. The R-band magnitudes of these stars range from 12 to 18. The bright end was constrained by the dynamic range of the CCD. Within the central 20% of the field (subject only 10 the R-filler) another hal f-dozen stars were detected that had expected photometric errors < 1%. These stars were used to calibrate against variability in atmospheric transmission. Of the total polarimetric sample, -50 sources had measured linear polarizations accurate to better than 3σ, or P/AP ≥ 3. The results of the polarization measurements for these stars arc given in '1'able 1. The coordinate positions arc accurate to 10- 15". The estimated photometric error of the V, R, I photometry is -10%. in Figure 1 (Plate 1) we plot the R-band polarization vectors for the Mon R2 Core sources. The E vectors arc overlaid on the R-band CCD image of the Mon R2 Core region. The length of the electric vectors is proportional to P. The large circle denotes the area of the field corresponding to the hole in the polaroid filters; stars located within the encircled area were used only for flux calibration. Also shown in the figure arc the I-band and K-band polarization vectors measured by. 1 lodapp (1987) for the central 3′ region of the cloud core (and located within our 'hole' area). The Mon R2 bipolar molecular outflow long-axis direction (Bally and Lada 1983) is indicated with arrows directed toward the north-west (blue-shifted gas) and south-east (red-shiflc(i gas).

in Mon R2 NW wc detected -170 and in Mon R2 NN -260 stars with S/N ratios >50:1. Within the central 20% of the NW field another 5 stars were detected that had expected photometric errors < 1%, while 7 were detected in the center of the NN field. Of the total polarimetric sample, -80 sources in the Mon R2 NW had measured linear polarizations accurate 10 better than 3σ, while

-45 were measured with this accuracy in Mon R2 NN. The result is of "the polarization measurements for the stars are given in Table 1. The R-band polarization vectors for the sources lota.ted in these" fields are plotted in Figure 2 (Plate II) and Figure 3 (Plate III). The E vectors overlay the R-band CCD images of the Mon R2 NW and NN regions, respectively.

3.1 The Polarization Mechanism

It is our goal to measure the component of starlight polarized by magnetically aligned grains in the Mon R2 molecular cloud. This operation is complicated by the fact that there are two additional components of polarized starlight that are both independent of magnetic fields. We consider two alternative polarization mechanisms: (1) polarization by scattering of starlight from interstellar dust associated with the extended Mon R2 cloud, and (2) intrinsic stellar polarization.

First we consider scattering by dust in Mon R2. With the local young stellar cluster providing the starlight and the dense filamentary gas structures acting as an efficient reflector, the dominant form of polarization is undoubtedly from a scattered component. Indeed, it is evident from our deep broadband CCD data that scattered light is plentiful in the Mon R2 core. However, it is not likely that the net polarization we measure has an appreciable scattered light component. Our method of measuring the polarization of stars relies upon a local background subtraction *via* aperture photometry. The typical size of a photometry aperture is -1 5", while the circular annulus used the for sky subtraction extends another 5". 'Thus, the scattered light measured in the aperture will exactly cancel the scattered light measured in the sky-annulus (unless there is a strong spatial gradient, over ≈ a few arc seconds in the scattered light). If, as we hypothesize, dust grains are magnetically aligned, then starlight passing through the cloud will be dichroically absorbed by the grains; the resulting polarization can be measured with respect to the local background radiation.

We have argued that our method is insensitive to diffuse-scattered light. Nevertheless, we are still vulnerable to highly polarized light from young stars associated with the star-forming cluster. The source of this polarization is probably due to local scattering from a dusty circumstellar/envelope

structure. Given that none of our 3σ detections are identified with IRAS point sources, our observations are probably not sensitive enough to detect very many of these (typically, heavily embedded objects. Next consider intrinsic stellar polarization in field stars. Intrinsic polarizations of up to 1-2% have been observed in late-type giants (cf. Dyck *et. al.* 1 W 1). As in the case of young stellar objects, the polarization mechanism is most likely related to scattering from an anisotropic media associated with the evolved star. Figure 4 shows the (a) degree and (b) angle of polarization distributions for the 3σ polarization detections (Table 1). Based on the large degree of polarization for the Mon R2 stars (see Figure 4), the relative contribution from evolved giants is essentially negligible, or at worst adds a small dispersion to the measured angle of polarization.

Finally, we expect few if any of the sources in Table 1 to belong to the stellar Population lying foreground to the Mon R2 cloud. Foreground stars should have very small (<1%) polarization since the line-of-sight extinction is most likely less than 1 A_v. Moreover, the extensive polarimetric measurements of Mathewson and Ford (1970) for stars near the Monoceros region (and thus representative of the field star population) generally do not show polarizations greater than 1%.

3.2 Polarization and Visual Extinction

In order to better understand the relationship between polarization *via* selective optical extinction of starlight and the intervening, aligned dust grains in the Mon R2 molecular cloud, we construct a polarization - extinction, P vs. A_v, relation. Extinction due to the molecular clouds was estimated for the three fields using the following: the method of star counts (see Bok 1956; Dickman 1978; Jarrett 1992) and the CO molecular gas column density. Both are briefly discussed below.

The R-band extinction was initially determined over squares 1.3' on a side; mean extinctions for larger slar-free regions were computed according to the prescription given by Dickman. All stars were treated as background objects. In principle, [his means that the *extinctions determined at each location in the cloud are only lower limits. In* practice, this simplifying assumption has varying impact on the results of interest depending on the actual Mon R2 extinction. For low opacity, $A_v < 2$,

w c expect more than 70% of the observed stars with R magnitudes brighter than 1 8 to be located behind the molecular cloud[7]. In relation to higher opacities, for example A_v - '5, the fraction of

[7] The stellar number densities arc estimated from a Galactic stellar distribution model (Jarrett 1992).

background stars is down to 20%. Consequently, the star count method is less effective for the heavily obscured regions of Mon R?..

Alternatively, a very good tracer of the dust extinction is the molecular gas column density. The gas column density is typically estimated from CO J = 1 - Ocmission line data. Xie (1992) estimated the visual extinction of the Mon R2 GMC using ^{13}CO column densities. The gas column densities were estimated from ^{12}CO and ^{13}CO (the latter was acquired by Bally, Langer, & Liu 1991) using the LTE method (Dickman 1978). Even though there is a fair amount of uncertainty in the absolute conversion 10 A_v, the relative extinction should be reliable for moderate to high opacities.

Given the strengths and weaknesses of the two methods described here, wc combine the extinction estimates accordingly: for $A_v < 2$, wc usc the star counts, and for $A_v > 2$, the molecular gas column density. The resultant visual extinction values range from 0.5 to 30 magnitudes. The relative extinction values corresponding to the stars with 3σ polarizations arc given in the last column of Table 1. Figure 5 shows the P vs. A_v relationship for the Mon R2 stars in "1'able 1. Also shown in Figure 5 is tile P/A ratio of 3, which is the upper limit observed for stars in the field (i.e., the diffuse interstellar medium; cf. Hiltner 1956). Although [here is a significant amount of scatter in the P 10 A relationship, there arc fcw points for which the ratio has a value much greater than 3, suggesting that the grain alignment mechanism in Mon R2 is probably similar 10 that functioning in the general interstellar medium. Consistent with this conclusion, the overall P-A trend seen in Figure 5 is that of increasing polarization with extinction, in which the peak polarization occurs for A_v - 3 - 4. For the heavily obscured regions of the Mon R2 fields the polarization appears to be decreasing or at least remain flat wiih increasing extinction. The scatter in the relation is aiso increasing wi(h extinction.

This result is consistent with other polarimetric studies of molecular clouds (cf. Vrba, Strom and Strom 1976). It has been hypothesized that the cause of this effect is related to the" dust grains themselves; namely, for dense regions the efficiency of polarization is lower relative to more diffuse areas. Clayton and Cardelli (1988), for example, have argued that the effect may be indicative of an increasing ratio of total-to-selective extinction, R_v, due to a grain population with increasing physical sizes *via* coagulation of small dust grains. On the other hand, Myers & Goodman (1991), Jones (1989), and Jones et al (1992), among others, have argued that the degree of polarization, as well as the dispersion in the direction of imlariz.alien, are influenced primarily by the line of sight column density of the polarizing dust grains and magnetic field geometry. An important assumption that these models adopt is that the magnetic field is composed of a uniform and random component. The basic idea is that as the starlight passes through the molecular cloud it encounters clumps of gas, Each of which is coupled to a nonuniform (or random) component of the ambient magnetic field. 'i'bus, there is a characteristic scale length corresponding to an opacity at which the random component of the magnetic field decorrelates. The flattening of P in Figure 5 may be indicative of a changing magnetic field geometry as the line of sight extinction increases, where the decorrelation opacity is ~3 - 4 A_V.

3.3 Polarization Field

'1'here are several notable features in tile polarimetry of the Mon R2 fields. In the cloud core (Figure 1), with the exception of the north-east quad rant, the average angle of polarization is 140 ± 25° (see aiso Figure 4b). '1'here is near alignment of the polarization vectors with the molecular outflow bipolar axis (at -140°) in both the south-east, 0 = 150 ± 31°, and north-west, O = 120 ± 29°, directions. Likewise, in lhc south-western quadrant the polarization vectors are aligned on average 145 ± 18°. The coincidence suggests a possible connection between the outflow and the cloud magnetic field (see §5). In contrast to these results, the north-east quadrant of the Mon R2 Core field exhibits E vectors that are aligned at position angle 30 ± 27°. This polarization is roughly coincident with a filament of dense gas that extends radially (at ~500" from the outflow center (see Xie, Goldsmith, &

Patel 1993). These R-band polarization results are consistent with the trend seen at smaller spatial scales in studies by Zaritsky *et. al.* (1987), who measured R-band polarization within a 9′ × 9′ region approximately centered on the core, and Hodapp's (1987) I-band and K-band polarization of the central core Of Mon R2 (the polarization vectors are shown in Figure 1).

With the exception of the north-east quadrant, the polarization results suggest that the ambient magnetic field corresponding to the Mon R?, cloud core region is directed at position angle 120 - 150° parallel with the major axis of the bipolar molecular outflow and roughly coincident with the galactic plane, at -155°. Whereas the polarization results of the north-east quadrant suggest that the ambient magnetic field geometry has been significantly modified with at least a 70° change in direction. Given the close proximity of a recent burst of high-mass star formation in the dense cloud core, the bent field morphology may be indicative of a "supercritical" mode of star formation (cf. Shu, Adams, & Lizano 1987). In addition to star formation, in §5 we consider the influence of a shock wave on the field geometry.

In the Mon R2 NW and NN regions (see Figures 2 & 3), the average angle of polarization is comparable to that of Mon R2 Core *at least along the western side of these fields* where $\theta = 153 \pm 34°$ for Mon R2 NW, and $\theta = 127 \pm 30°$ for Mon R2 NN. The coherency of the polarization vectors appears to decrease in the north-eastern quadrant of Mon R2 NW, and in the eastern half of the Mon R2 NN field. Most of the stars in these areas have polarizations less than 1%. An opaque ridge of gas bisects the NW field and diagonally crosses the NN field. Within the narrow dust ridge itself, our R-band observations were not sufficiently deep to detect stars located behind this feature or their polarizations. To the east of the ridge, corresponding to a region of apparently lower extinction, there are very few stars with measurable polarizations. Nevertheless, the eastern ensemble of stars with $\geq 3\sigma$ polarizations has an average vector direction $20 \pm 56°$ in the NW field, and $93 \pm 43°$ in the NN field, roughly *parallel to* the ridge (at ~00 in NW and 60° in NN). To the west of the opaque ridge, the extinction appears to be relatively greater than to the east and there are considerably more stars with 3σ polarizations; note however, the typical degree of polarization in the NN field is roughly a factor

of two less than that of the NW and Core fields (see Figure 4a), which in all probability relates to a dust opacity gradient extending radially from the core. The combined polarization results suggest that the ambient magnetic field threads the western side Mon R? GMC at a projected angle between 12'() and 1600. Along the eastern side, the results suggest (at least in the Core region) that the field has been modified by some combination of gravitional collapse and shock compression. In the next section we discuss this scenario.

4. Discussion

It is evident that the inferred magnetic field structure of Mon R2 is far from simple. Polarimetry of the three CCD fields presented in Ibis work reveals an overall structure common to each field and consistent with the local Galactic magnetic field, but with significant differences. These nonuniformities are related to both small-scale changes in the gas associated with massive star formation, and (o the large-scale alteration of the cloud geometry by a shock compressed gas shell. For the sake of clarity, we consider these domains separately in the following discussion.

4.1 SnEill-Scale Field Structure

The "core" region -. the location of one of the most energetic and complex bipolar outflows observed in molecular clouds and the silt of recent high-mass star formation -- is characterized by a significantly distorted field structure. This distortion appears to originate from the dense cloud core (1 Iodapp 1 987) and extends out to the boundary of the core region. It has been hypothesized by Hodapp (198-/) that this distortion of the magnetic field structure is due to the effects of gravitational contraction along the ambient magnetic field axis and cloud rotation. As the dense asymmetric core forms, the magnetic field lines, which are frozen into the gas, bend toward the center of the structure. Our polarimetric data supports this physical scenario to the extent that the large scale magnetic field is roughly perpendicular (± 200' to the long axis of the inner core region and to the bent field geometry.

Although the magnetic field is probably not a dynamically dominant component in the recent star . . . formation, it is likely that the field played an important role in slowing the gravitational collapse, and correspondingly, in [tic form of the stellar mass function. As noted in the review by Shu, Adams, and I .izano (1987), in supercritical cloud collapse, the magnetic forces arc overwhelmed by the cloud gravitational forces resulting in a bending of the magnetic field, and subsequently, amplification of the field strength. The tension between the magnetic field lines tend to oppose the inward fall of gas (which is dragging the field with it) so that the gravitational collapse is effectively '(diluted".

"1'here are a number of factors that potentially confuse the simple picture described above. These arc all related to the fact that the physical environment of the Mon R2 cloud core is far from quiescent (as was once thought). in addition to turbulent gas motions, the dense core of Mon R2 possesses a massive bipolar molecular outflow, -1047 ergs (Bally and Lada 1983), by far the dominant energy source in the core. An outwardly radial-directed wind from the young object may transfer enough energy to the local surrounding media that it functions as tbc dominant form of cloud support (relative to gas turbulence or the magnetic field). The coincidence between the projected magnetic field structure and the bipolar' axis suggests that the outflowing gas from this object is preferentially *expanding* along the magnetic field -- which is also coincident with the direction of the largest density gradient. Furthermore, the 70° change in the angle of polarization observed in the north-east quadrant of Figure 1 (which wc interpret as a twist in the magnetic field) appears to trace a toroidal gas structure (cf. Torrelles et al. 1983) associated with the protostellar object. The toroid is perpendicular to the bipolar outflow axis (Xie and Goldsmith 1993). This result has also been observed in other young stellar objects; for example, Aitken et al. (1993) observed that the angle of polarized infrared light as seen through the densest regions of high-mass protostellar objects tends to be perpendicular to the outflow axis and coincident with the plane of their toroidal disks. It should be noted that wc see no evidence in our polarimetric data for a toroidal structure along the south-west direction of the bipolar outflow, which by symmetry should be opposite to the north-east feature (see Figure 1). This

null result may be related to jrlcli[ult.jell effects (the outflow is inclined ~70° relative to the line of sight) and to the large extinction; $A_V >> 1$ (). near the core (Xie 1"992)."

As previously discussed in §3.2, the correlation between the observed polarization and the magnetic field geometry is complicated by the fact that the opacity in this region is both large and clumpy. As seen in the R-band images, there are many dark clumps and filaments observed in projection across the Mon R2 field, and presumably, there are clumps situated along the line of sight. Thus, we are effectively measuring the integrated dichroic absorption of starlight through different magnetic field geometries along the line of sight. If the magnetic field decorrelation length is something like 1 A_v (as suggested by Jones et **iii.** 1 992) [hen the polarized light we measure should represent several different field directions and the dispersion in the angle of polarization should be correspondingl y high (primarily duc to the nonuniform component of the magnetic field; cf. Myers & Goodman 1 991). in this extreme case, the polarization is more representative of changing opacity (in combination with the underlying magnetic field geometry) than a direct measure of the magnetic field structure. Instead of a "bent" magnetic field morphology, the complex polarization in the north-cast quadrant of the Core field (Figure 1) may instead reflect the complex clumpy gas structure in this area, Empirically, however, we find that the dispersion in the angle of polarization is small for this field, which implies that the polarization is tracing a uniform magnetic field structure. Also, the degree of polarization to extinction relation (Figure 5) crudely suggests that the decorrelation opacity is somewhat larger, more like ~3 - 4 A_v (as discussed in §3.2). in this case, the optically polarized light traverses at most two uncorrellated magnetic field geometries; consequently, the expected dispersion in the angle of polarization should be small - our polarimetric results are more compatible with this less extreme case.

4.2 Large-Scale Field Structure

Recent observational results at mm wavelengths reveal an expanding gas-shell now dominates the Mon R2 GMC (Xie 1992; Xie, Goldsmith & Patel 1993). The expanding gas bubble is immense,

.-3: in diameter (crossing time of. ~10^7 years), with a projected center (origin) ~30′ east of the cloud core and located behind the bulk of the Men"]{? cloud. The estimated mechanical energy of the shell, is 1 0^{49} ergs. The western front of the bubble shell, corresponding to high-density gas > 1 0^4 cm^{-3} moving at 3.5 -4.5 km/s (VLSR - 11 - 14 km s"]), is clearly seen as an opaque ridge in our Mon R2 NW and NN fields (Figures 2 and 3). The authors suggest that the main central core, including the outflow and embedded stellar cluster, forms a "peninsula" structure extending into the cavity or postshock region (see Figure 1). The cavity side, oriented toward the east relative to our three polarimetric fields, is characterized as a hot low density medium with H_2 densities less then 100 cm^{-3}. The eastern side of Mon R2 NN (Figure 3) best illustrates the low extinction cavity region.

The radio data provides clear evidence that the large scale gas structure of Mon R2 has undergone asymmetric compression. Since the magnetic field is frozen into the gas, tile B field geometry should also be modified by the expanding shell. In addition, shock waves can alter the velocity field and can deposit energy into the medium - either of these two mechanisms can result in a distorted field in the post-shock region. We may explore this possibility by comparing the polarimetry in the three fields with the corresponding molecular gas morphology. Figure 6 shows a grey-scale rendering of tile ^{12}CO J = 1 -0 peak antenna temperature for the Mon R2 core and vicinity. Also indicated in Figure 6 are the three polarimetric fields, Core, NW and NN (denoted by large boxes) and their corresponding E vectors. It can be seen that a curving ridge of dense gas extends northward from the core (southernmost box) through the center of the NW field and through the eastern side of the NN field. Figure 6 compactly illustrates the coherent magnetic field structure along the western side of the CCD fields with an average direction -1200 to 170°, which is roughly coincident with the local Galactic magnetic field -- as is true for the global field in the Galactic disk. The gas kinematics are rather complicated near the western shock front of Mon R2 (partly due to projection effects), and tires it is not clear if any of the regions to tile west of the opaque dust ridge (which we identify as the expanding shell) have been affected by the compression wave. Consequently, we cannot unambiguously conclude that the coherent magnetic field threading tile gas in

the western region of our CCD fields represents the ambient primordial field of Mon R2. . . . Nevertheless, *it is remarkable that the larger part of the magnetic field in Mon R2 appears to be azimuthal with the Galactic plane.* This result is in accordance with the Parker instability (Parker 1966), where molecular clouds weigh down the magnetic field and constrain its structure along the plane Of the Galaxy. Curiously, this is not seen quilt so clearly in Orion (Vrba, Strom & Strom 1988), another giant molecular cloud often connected with Mon R2 due to their unusually large dislocation from the galactic plane. Sonic authors (cf. Franco et al 1988) have proposed models explaining the common origin of the Mon R2 and Orion giant molecular clouds, while also directly or indirectly relating this "event" with that of Gould's Belt. Notwithstanding the complexity of Orion's magnetic field structure, the coincidence of the magnetic field direction in Mon R2 and the Galactic plane direction is significant and needs to be investigated in other GMCs. In the following discussion, we adopt 150° as the nominal sky-projected ambient magnetic field direction.

In its simplest form, magnetic field distortion resulting from ii shock wave depends on the angle between the ambient field direction and the shock front. The component of **B** parallel to the shock front is compressed and amplified, while the orthogonal component dots not change. The shock front of the gas shell expanding into the western portion of Mon R2 appears to be inclined roughly 40-50° to the **B** field in the NW and NN regions, and perhaps 10-2.00 to the ambient field in the Core region. If our interpretation of the geometry is correct, [hen we would expect a distortion in the ambient magnetic field counter-clockwise from 150° - however, it must be emphasized that the magnetic field geometry inferred from linear polarization is limited to the two-dimensional plane of the sky. Based solely on the geometry, the largest measurable distortion should be in the NN region, followed by the NW region, and finally the Core region. Given the complexity of the clorrct/shell geometry, as well as our very simplistic approach, we acknowledge that the scenario described here may be largely in error, particularly for the southern most fields (Men R2 Core). Indeed, as already noted there appears to be significant distortion in the magnetic field within Mrm R2 Core, in which the polarization vectors corresponding to the north-cast quadrant *arc* inclined -7010 the rest of the Core

region. Rather than any single dominating factor, the bent field morphology "is most likely the combined result of gravitional collapse and a vectored (asymmetric) force.

In contrast to the well-defined Core E vector orientation, the polarization results for the eastern side of the NW and NN field -- corresponding 10 the evacuated side of the expanding shell - is characterized by stars with relatively low percentage of polarization and, significantly, a nearly incoherent distribu tion of electric vectors. The low percentage of polarization in the NN region is due 10 the relative paucity of gas and dust ($A_v < 2$), since most of it has been swept up by the expanding bubble shell. Unfortunately, this circumstance means that foreground interstellar clouds situated along the line of sight can have comparable polarizations to that of the molecular cloud itself. For example, if the extinction foreground to Mon R2 (d - 850 pc) is -().6 A_v, then the degree of polarization duc to foreground clouds can bc as large as -().9 - 1%. The end effect is a large dispersion in the angle of polarization. In addition to foreground cloud contamination, hot and turbulent gas in the post-shock region may also contribute to a large dispersion in 0. Our data appears to confirm these suspicions: for the eastern half of the NW and NN regions wc find O = 10 ± 56° and 95 ± 43°, respectively. In **other** words, the dispersion along the eastern side of the Mon R2 fields is roughly twice as large as that measured for the western side. Notwithstanding the large dispersion in 0, the average angle of polarization suggests that the magnetic field has undergone a counterclockwise distortion of -40-60°.

At this point wc draw attention to an important polarization feature in the NW field. The average angle of polarization for the sources located in the south-west quadrant of Mon R2 NW is 173 i 23, which is offset -25° counter-clockwise from the nominal **B field** direction (see Figure 2 and 6). In accordance with the preceding (discussion, this result suggests that the gas in this quadrant is part of **the shock** compressed shell. The ^{12}CO observations (Figure 6) and particularly, the ^{13}CO gas column densities (Xie 1992) arc consistent with this conclusion. The polarization vectors just to the south of **this** quadrant (and slightly east, corresponding to the nor[h-west quadrant of Mon R2 Core) arc aligned at 120 ± 29°. *As traced by [he gas and magnetic field, wc appear to be viewing the projected curvature in the shock compressed shell.* If this is indeed the case, then it must be that nearly all of

the gas within the three CCD 'fields 'is postshock or at least part of the expanding shell. It then " . . . . follows that the coherent magnetic-field structure inferred from our polarimetry may not be truly . . representative of the ambient (preshock) magnetic field geometry. Additional polarimetric measurements of fields located to the west of the expanding shell are necessary in order to verify our conclusion that the ambient magnetic field is directed at position angle -1500 A future KPNO date has been scheduled in order m carry out this project.

4.3 Combined Field Structure

in the context of an energetic shock wave propagating through the Mon R2 giant molecular cloud, the magnetic field tines have been distorted by the expanding shell leaving a compressed or swept-up magnetic field structure near the interface. A possible outcome of just such a distortion, which includes amplification in the magnetic field, is local clumping of the gas and subsequent gravitational collapse. This may have recently occurred in the Mon R2 complex. Aligned along the northern gas ridge, in the post-shock region, there arc [ens of IRAS points sources which arc presumed to be deeply embedded young stars (Xie 1992.). in contrast, there arc few IRAS point sources along the western side of the GMC. The location and age of these sources suggest shock-triggered star formation, and to which wc conclude that the primary form of cloud support beyond the dense core, the magnetic field, has been significantly altered. This mode of star formation is certain to be common throughout the Galaxy. in a polarization study of the CMa R1 association, for example, Vrba, Baierlein & Herbst (1987) similarly find that the underlying magnetic field has been distorted by a shock wave. In the case of CMa R], a proximal supernova provides the vectored force that distorts the ambient B field and triggers a burst of star formation interior to the "amplified" magnetic field. Both in Mon R2 and CMa R 1, a large scale structure has significantly altered the cloud environment, from the largest size scales, in which we observe filamentary gas morphology and curvature in the ambient magnetic field geometry, 10 the smallest, in which wc detect local clumping of gas and recent star formation events.

As a final caveat, we remind the reader that our polarimetric measurements and subsequent interpretation of the magnetic field structure is limited to the plane of the sky. Given the energetics of Mon R2 and complications due to the massive bipolar outflow and expanding bubble shell, it remains a very difficult task to understand the magnetic field geometry. Nevertheless, the results of this study, in concert with those of the central Orion A molecular cloud (Novak *et al* 1989), suggest that magnetic fields are an important component to massive star formation regions.

6. Summary

We have carried out polarimetric observations to study the magnetic field structure of the Mon R2 giant molecular cloud. The polarimetry was calibrated using a new technique that relies on obtaining photometry of stars simultaneously with polarimetric photometry of object fields, thus providing an accurate means to measure the polarization of electric vectors for stars observed through the Mon R2 cloud. The main points and conclusions of this work may be summarized as follows:

- We obtained deep R-band CCD polarimetry of three fields located towards the Mon R2 molecular cloud, covering a total area of 0.5 square degrees. The polarimetry was complete for all stars brighter than R ~ 18, comprising more than 600 stars. Of this total, ~170 stars had measured polarizations with $\geq 3\sigma$ accuracy.

- The polarizations for sources observed through the Mon R2 molecular cloud have values consistent with selective extinction *via* a grain alignment mechanism similar to that functioning in the general interstellar medium. The overall trend is of increasing polarization with extinction, up to $A_v \sim 3$, at which the polarization appears to be decreasing or at least remain flat with increasing extinction. One possibility is that for the dense regions, the efficiency of polarization is diminished in comparison to that of more diffuse areas. Another possibility is that the magnetic field geometry changes according to the number of gas clumps along the line

of sight as measured from the total line of sight opacity. In this case, the characteristic decorrelation opacity is $\sim 3 A_V$.

- The Mon R? "core" magnetic field structure is comprised of three distinct features as inferred from the polarization vectors: general alignment parallel to the long axis of the cloud filament, coincidence with the bipolar molecular outflow axis and the local Galactic magnetic field, and finally, distortion or bending toward the long axis of the cloud core. The latter two features suggest that magnetic fields play an important role in massive star formation regions. in addition to gravitational and rotational stresses, another mechanism that contributes to the distorted magnetic field is an energetic shock wave, which recent mm-wave observations reveal is now dominating the Mon R2 complex.

- The polarimetry suggests continuity between the northern and core general magnetic field structure. The mean angle of polarization for stars located along the western side of the three CCD fields is -150 ± 35°, which is roughly coincident with the local Galactic magnetic field. To the north of the Mcrn R2 core region, the polarization vectors exhibit an increasing erosion in coherency as seen from west to east across the CCD fields. These CCD fields are bisected by a dense ridge of gas which appears to be the boundary of a shock compressed shell. Our polarimetry suggests that the expanding shell has distorted the magnetic field lines extending from the core to the northern gas structure comprising Mon R?.. One possible consequence of the shock-altered magnetic field is a recent burst of star formation along the eastern boundary of the gas ridge.

Acknowledgements

We would like to thank Dave Silva and George Jacoby for their onsite technical support at Kitt Peak National Observatory. THJ would like to thank Mark 1 Ieyer, Mike Meyer and Steve Strom for their helpful comments. This work was carried out in part at the Jet Propulsion Laboratory, California Institute of Technology, under a contract with the National Aeronautics and Space Administration.

References

Aitken, D.K., Wright, C.M., Smith, C.H., & Roche, P.F. 1993, MNRAS, 262, 456.

Aspin, C., & Walther, D.M. 1990, A&A, 235, 387.

Bally, J., Langer, W.D., & Liu, W., 1991, ApJ, 383, 645.

Bally, J., & Lada, C.J. 1983, ApJ, 265, 824.

Beckwith, S., Evans, N. J., Becklin, E.E., & Neugebauer, G. 1976, ApJ, 209, 390.

Bok, B.J. 1956, AJ, 61, 309.

Clayton, G.C. & Cardelli, J.A. 1988, AJ, 96, 695.

Davis, L., & Greenstein, J.1. 1951, ApJ, 114, 206.

Dickman, R.L. 1978, AJ, 83, 363.

Dyck, H. M., & Lonsdale, C.J. 1979, AJ, 84, 1339.

Dyck, H. M., Forbes, F. F., & Shawl, S.J. 1971, AJ, 76, 901

Eggen, O.J. & Sandage, A. R. 1964, ApJ, 140, 130.

France, J., Tenorio-Tagle, G., Bodenheimer, P., Rozyczka, M., & Mirabel, I.F. 1988, ApJ, 333, 826.

Gillis, J., Mestel, L., & Paris, R.B. 19"/4, A& ASS., 27, 167.

Goodman, A. A., Bastien, P., Myers, P.C., & Menard, F. 1990, ApJ, 359, 363.

Hackwell, J. A., Grasdalen, G.L., & Gehrz, R. 1982, ApJ, 25?., 250.

Heiles, C., Goodman, A. A., McKee, C., & Zweibel, E.G. 1991, in IAU Symp. 147, Magnetic Fields in Star-Forming Regions.

Herbst, W. & Racine, R. 1976, AJ, 81, 840.

Heyer, M.H., Snell, 1{.1.., Goldsmith, 1'.1'., Strom, S.E., & Strom, K.M. 1986, ApJ, 308, 134.

Hildebrand, R.H. 1988, QJRAS, 29, 327.

Hiltner, W.A. 1956, ApJS, 2, 389.

Hodapp, K.W. 1984, A&A, 141, 225.

Hodapp, K. W. 1987, A&A, 172, 304.

Jarrett, '1'.11. 1992, Ph.D. Thesis, University of Massachusetts.

James, K.A. & Smith, G.H. 1984, AJ, 89, 487.

Jones, ' 1 ' . 1 . 1989, ApJ, 346, 728.

Jones, 'l'. J., Klebe, D., & Dickey, J.M. 1992, ApJ, 389, 602.

Kutner, M.],. & Tucker, K.D. 1975, ApJ, 199, 79.

Landolt, A.U. 1983, AJ, 88, 439.

Lee, H.M. and Draine, B.T. 1985, ApJ, 290, 211.

Loren, R.B. 1977, ApJ, 215, 129.

Maddalena, R. J., Morris, M., Moscowitz, J., & Thaddeus, P. 1986, ApJ, 303, 375.

Mathewson, D.S. & Ford, V. L. 1970, MeMRAS, 74, 139.

Mouschovias, T. CH. 1978, in Protostars and Planets, ed. 'l'. Gehrels, Tuscon: Univ. of Arizona Press, p. 209.

Myers, P.C. & Goodman, A.A. 1988, ApJ, 326, L27.

Myers, P.C. & Goodman, A.A. 1991, ApJ, 373, 509.

Myers-Rice, B.A., & Lada, C.J. 1991, ApJ, 368, 445.

Novak, G., Gonatas, D.P., Hildebrand, 1<.11., Platt, S.R., & Dragovan, M. 1989, ApJ, 345, 802.

Novak, G., Predmore, C.R., & Goldsmith, P.F. 1990, ApJ, 355, 166.

Novak, G., & Jarrett, T.H. 1993, J. Applied Optics, submitted

Parker, E.E. 1966, ApJ, 145, 811.

Sate, S., Tamura, M., Nagata, 'l'., Kaifu, N., Hough, J., McLean, 1. S., Garden, R.P., & Gatley, 1. 1988, MNRAS, 230, 321.

Serkowski, K. 1974, l'olari~.alien Techniques, in Methods of Experimental Physics, 12A, ed. N. Carleton, New York: Academic Press, p. 348.

Shu, F.]]., Adams, F.C., & Lizano, S. 1987, ARA&A, 25, 23.

Shu, F.H., Lizano, S., Adams, F. C., & Ruden, S.P. 1988, in Formation anti Evolution of Low Mass Stars, eds. Dupree, A.K. & Lago, M.'i'.V."l"., Kluwer, Dordrecht, p. 123.

Strom, K. M., Strom, S.E., Wolff, S., Morgan, J., & Wenz, M. 1986, ApJS, 62, 39.

Thronson, 11. A., Gatley, 1., Harvey, P. M., Sellgren, K., & Werner, M.W. 1980, ApJ, 237, 66.

Torrelles, J.M., Rodriguez, .F., Canto, J., Carral; P., Marcaide, J Moran, .M. & Ho ?T.P 983, ApJ, 274, 214.

Vrba, F.J., Baierlein, R., & Herbst, W. 1987, ApJ, 3 7 >07.

Vrba, F.J., Strom, S.E., & Strom, K.M. 1976, AJ, 8 , 958.

Vrba, F.J., Strom, S.E., & Strom, K.M. 1988, A , 96, 680.

Xie, T. 1992, Ph.D. Thesis, University of Massachusetts.

Xie, T., & Goldsmith, P.F. 993, ApJL, submitted.

Xie, T., Goldsmith, P.F., & Patel, N. 1993, ApJL, in press.

Zaritsky, D., Shaya, E.J., Scoville, N.Z., Sargent, A.I., & Tytler D. 1987, AJ, 93, 1514

Figure Captions

Figure 1 (Plate I) R-band polarization vectors corresponding Jo Table 1 sources overlaid on R-band CCD image of the Mon R2 Core region. The length of the electric vectors is proportional to I'(%). The large circle denotes the area **of** the **field** corresponding 10 the hole in the polaroid filter. The I-band and K-band polarization vectors (} lodapp 1987) for the central 3′ region of the cloud core arc also sh10WI1. The Mon R2 bipolar molecular outflow long-axis direction (Bally and Lada 1983) is indicated with arrows directed toward the north-west (blue-shif[ed gas) and south-cast (red-shifted gas).

Figure 2 (Plat e 1 I) R-band polarization vectors tori esponding to '1'able 1 sources overlaid on R-band CCD image of the Mon R2 NW region. The sym bo]s used arc described in Figure 1.

Figure 3 (Plate 111) R-band polarization vectors corresponding to "1'able 1 sources overlaid on R-band CCD image of the Mon R2 NN region. The symbols used arc described in Figure 1.

Figure 4 (a) Distribution of degree of polarization, P(%), and (b) angle of Polarization, θ (degrees), for the Mon R2 sources ('I'able 1) given as histogr ares.

Figure S Percentage polarization versus visual extinction for stars observed through the Mon R2 cloud ('I'able 1). Also indicated is the P/A upper limit observed for field stars observed through diffuse interstellar clouds.

Figure 6 ^{12}CO J = 1 -0 peak antenna temperature for the Mon R2 core and vicinity. The temperature (and grey-scale) ranges from 1 to 1 5 K; contour levels correspond [o 4 and 8 K. The greyscale is overlaid by the polarization vectors of the three fields observed in this study, Core, NW, and NN regions, from southtonorth.

TABLE 1

Mon R2 Linear Polarization Measurements for Stars with P/ΔP ≥ 3

α (1950) hh mm ss	δ (19s0) dd mm ss	V	R_C	I_C	P %	ΔP %	θ	Δθ	A
060540.4	-63340	17 .3	16.1	1s.2	3.3	0.9	139.4	8.7	1.6
06 0141.9	-633 12	16.1	14.3	12.9	5.7	0.3	14s.6	1.3	6.0
060140,4	-63238		17.4	]5,9	10.5	2.0	150.0	6.4	6.S
06 0503.9	-63228	16.4	15.4	14.5	4.0	0.7	131.3	5.9	6.4
06 04 38.9	-63227		15.8	14.4	().x	0.8	156.3	3.1	7.4
06 04 34.1	-632 15		16.2		4.7	().7	166.5	3.3	7.0
0605 44.S	-63213		17.3	16.4	6.S	2.2	106.()	11.1	3.6
060140.6	-632 OS	15.s	15.1	14.5	1.6	().5	156.6	7.5	7,s
060533,4	-63150	16.5	15.4	14.4	1.9	(),4	143.3	3.8	3,9
06 06 03.1	-63132	16.5	15.7	15.0	23	0.7	129.9	9,9	1.5
060544.9	-631 1X		17.3	16.3	8.1	?.7	138.9	12.5	3.4
0601 5?.3	-63036		16.8	15.9	5,1	1.1	145.2	3,1	5.0
060521,6	-62901		16.7	15.4	3,8	1.0	163,S	8.8	6.S
06 04 51.6	-62855	17.5	16.0	14.6	2,9	0.6	134.3	5.8	9.2
060501,0	-6 2S 46	..	1"/.3	16.4	5.0	1.6	149.8	7.s	2.4
060600,3	-628 25	17.2	16.3	]5.4	4.()	0.7	131.7	2.8	2.6
060555.2	-628 () ()	...	17.6	16.8	11.3	2.0	7.7	3.()	4.8
060557.7	-62644	16.9	15,2	13.7	4.2	0.4	129.2	1.9	4.6
060135.9	-6 26 () ()	.	15.6		2.6	0.4	165.1	4.2	3.0
060546.8	-6 2s 36	16.6	15.4	14.3	1.6	0.5	46.2	8.1	9.5
06 04 50.7	-62525	...	16.9	15.8	3.5	1.1	131.6	8,7	9.1
060141,9	-6 2524	15.6	14.6	13.8	2.2	0.3	144.6	2.-1	3,2
060143.9	-62523	...	16.S	15,]	4.2	0.9	153.0	6,6	4.6
060143.0	-624 6(I	16.7	15.4	14.3	2.8	(),4	147.4	2.5	3.2
06 04 36.5	-62338	16.0	15.2	14.6	1.3	().4	88.8	7.1	0.9
060451,8	-6231S	16.0	15s)	14.1	0.9	0.3	141.2	7.8	3.4
0605 S4.3	-62052	16.6	15.4	14.4	1.8	0.4	90.0	6.2	5.8
060545.5	-62037		16.3	14.8	2,9	0.7	168.7	7.6	5.1
06 04 3s.1	-620 18	...	15,2	...	1.5	0.4	97.4	7.9	5.2
060541.5	-61842	17.6	16.6	15.-1	4.6	1.4	46.1	10.5	9.0
060136.2	-61838		16.5	15.3	3.5	0.8	133.9	4.4	3.3
060553.9	-61810	17.3	16.1	15.1	2.1	0.6	63.3	7.s	4.6
06 04 3S.8	-6 16 30	...	16.6	15.1	4.6	1,3	132.0	11.3	4,9
060528,1	-61630	17.8	16.0	14.6	4.3	(),6	4,7	4.4	3.5
060146.4	-616 2s	17.7	15.5	13.8	4.6	().5	131.3	2.3	5,6
060551.2	-61626		16.4	15.1	9.2	0.8	56.2	1.9	5.6
060521.0	-6 1555		17.3	15.s	6.8	2.0	61.2	8.2	9.s
060556.7	-6 15 19	.	16.8	14.9	8.9	1.(J	33.1	1.2	3.5
(k') 05 2X,3	-61501	17.2	15.9	14.7	4.()	().5	1 0.8	2.0	1.4
060523,4	-61427	14.7	13.8	12.9	4.8	0,3	33.6	().9	3.s
060527.9	-6 14 18	14.6	13.8	13.0	4.1	0.3	6.8	2.5	1.1
060545,9	-6 14 08	16.8	15.5	14.4	2.3	0.5	23.0	5,5	().7
060544.3	-6 1348	16.4	14.9	13.7	2.3	0.3	178.0	5.4	().6
06 05 27.6	-61329	16.8	15.-/	14.8	4.3	0.5	15.9	2.3	0.9
060527.6	-6 12 48	..	16.7	15.5	4.2	1.0	40.7	6.7	1.0
06 0149.-I	-6 12 38	15.6	14.0	12.6	2.7	0.3	147.9	2.5	3,2
0601 (19.1	-61655	..	16.4		3.5	0.4	172.3	I.8	7.3
060137.9	-('1 1621	18.5	16.6	15.1	3.4	().4	123.7	2.8	4.6
060.1 4S.5	-6 16 18	17.7	15.6	13.9	4.6	(),3	132.1	1,6	5.6
06 04 13.0	-6 16 09	17.0	15.6	14.4	1.7	(),3	160.3	4.6	5,9
06 0453.()	-61544	19.6	18.1	16.5	4,7	1.5	145.1	7.4	6.6
0605 16.7	-61537	...	18.0	...	4.6	1.5	175.s	7.6	9.0
0601 1(1.3	-6 15 18	19.8	17.5	15.9	7.6	1.2	158.4	4.4	5.9
0601 19.4	-61 502	18.4	17.2	16.0	5.8	().8	155.1	3,8	3.7
060101.5	-6 14 () ()	18,6	16.s	15.3	4.3	().6	161.4	3.4	2.8
060501.2	-61334	17.5	16.6	15.7	3.0	0.7	157.5	6.2	3.1
06 ().3 50.8	-61332	15.0	14.4	13.8	0.8	(),'2	35.3	3.7	().8
060404.8	-6 1329	18.4	16.8	15.5	7.0	0.5	167.3	0.9	3.3
06 04 09.7	-61313	18.4	17.1	16.1	5.()	(),6	160.6	2.0	4.2
060351,7	-61253	14.8	13.4	12.1	1.9	0.2	169.5	4.1	1.1

TABLE 1- *Continued*

α (1950) hh mm ss	δ (1950) dd mm ss	V	R_C	I_C	P %	ΔP %	θ	Δθ	A_V
06 04 06.7	-6 12 40	...	18.2	...	4.8	1.6	168.5	9.6	3.6
06 04 48.8	-6 12 28	15.6	14.0	12.6	2.5	0.2	148.4	1.9	2.5
06 04 06.8	-6 12 23	14.0	13.4	12.9	0.6	0.2	8.1	8.5	3.7
06 04 19.5	-6 12 22	18.0	17.0	16.1	3.5	0.6	158.1	4.1	4.0
06 04 56.8	-6 11 31	17.3	15.8	14.2	1.6	0.3	90.3	3.3	3.7
06 04 05.0	-6 11 24	18.0	16.7	15.3	6.4	0.5	167.7	1.0	4.5
06 04 09.6	-6 10 42	18.9	16.6	14.7	8.2	0.4	162.4	1.0	7.0
06 03 50.3	-6 10 17	18.8	17.6	16.4	3.5	1.1	143.6	6.6	1.0
06 03 52.0	-6 09 52	14.1	13.5	13.0	0.6	0.2	46.2	8.3	1.0
06 05 12.5	-6 08 32	15.7	15.0	14.5	0.9	0.2	77.1	3.2	5.6
06 03 50.9	-6 08 24	17.5	16.2	15.0	2.6	0.4	158.6	3.9	0.7
06 04 11.5	-6 08 20	17.7	15.9	14.3	5.7	0.4	164.1	1.9	5.1
06 05 12.3	-6 07 49	16.7	15.6	14.6	0.9	0.3	79.2	8.4	4.9
06 04 00.8	-6 07 49	14.2	13.6	13.1	0.6	0.2	61.2	8.2	3.2
06 03 57.7	-6 07 42	16.9	15.5	14.3	3.1	0.3	166.4	2.3	2.5
06 05 11.2	-6 07 41	14.3	13.6	13.1	1.0	0.2	90.3	3.6	4.9
06 03 53.4	-6 07 35	16.0	15.1	14.3	2.4	0.2	174.8	1.8	1.9
06 03 49.9	-6 07 31	18.5	17.2	16.4	2.2	0.7	173.5	5.3	1.7
06 05 20.0	-6 07 29	16.9	15.9	15.2	1.2	0.3	86.8	5.5	4.3
06 05 16.2	-6 06 55	...	17.8	16.5	4.7	1.3	17.2	7.6	4.1
06 04 05.4	-6 06 35	18.9	17.5	16.2	3.5	0.9	163.0	6.8	2.7
06 03 55.3	-6 05 46	19.8	17.5	16.1	3.4	0.9	173.2	5.7	4.3
06 04 00.8	-6 04 34	15.3	14.6	14.1	0.6	0.2	54.7	5.2	2.9
06 04 14.4	-6 04 01	...	18.2	...	4.8	1.6	163.9	5.2	3.0
06 03 56.1	-6 03 59	18.2	16.6	15.3	2.5	0.8	0.3	4.3	2.1
06 05 00.0	-6 03 17	18.9	17.3	16.1	3.0	0.8	158.0	5.4	3.7
06 04 06.4	-6 03 10	18.2	17.2	16.1	4.5	0.9	162.5	6.6	2.6
06 05 12.6	-6 03 02	13.9	13.3	12.8	0.6	0.2	92.0	6.0	3.6
06 04 56.7	-6 01 52	17.1	15.5	14.1	3.5	0.4	171.6	1.6	0.5
06 03 51.7	-6 01 48	16.6	15.6	14.6	1.6	0.2	159.1	2.8	2.2
06 03 52.1	-6 01 32	19.0	17.4	16.4	2.8	0.9	154.5	9.2	2.5
06 04 07.4	-6 01 21	18.8	17.1	15.9	2.4	0.7	147.8	9.6	2.8
06 05 03.4	-6 01 01	18.8	17.8	16.8	3.3	1.1	4.4	7.5	1.9
06 04 21.6	-6 00 25	16.5	15.5	14.7	1.5	0.3	146.7	4.7	2.4
06 04 22.7	-6 00 14	17.4	16.4	15.6	3.1	0.4	145.7	2.6	3.0
06 04 12.6	-6 00 11	18.7	17.6	16.7	3.7	1.0	136.4	9.6	3.6
06 04 39.1	-6 00 10	16.7	15.8	15.0	1.6	0.4	110.4	6.6	6.2
06 04 58.7	-6 00 00	16.8	15.3	14.0	1.6	0.2	161.9	3.8	2.7
06 04 32.7	-5 59 56	16.0	15.4	14.8	1.4	0.2	94.4	2.9	4.6
06 04 31.4	-5 59 38	17.8	16.7	15.4	1.9	0.5	101.9	7.2	4.8
06 04 12.4	-5 59 18	16.9	15.9	15.2	1.1	0.3	87.1	7.1	3.4
06 04 18.5	-5 59 14	18.1	17.1	16.1	2.6	0.6	148.0	6.9	1.4
06 04 09.5	-5 59 11	18.8	17.5	16.3	3.8	0.9	145.1	5.7	3.2
06 03 57.1	-5 58 40	16.1	15.3	14.6	0.9	0.3	85.3	10.1	4.6
06 05 17.0	-5 58 09	15.9	15.2	14.6	1.2	0.2	97.7	3.7	3.3
06 04 15.1	-5 58 08	18.3	17.2	16.2	2.3	0.7	143.1	6.8	1.8
06 04 05.2	-5 58 08	17.6	16.6	15.5	3.3	0.4	151.9	2.9	2.4
06 04 55.2	-5 57 57	...	18.2	...	6.5	1.6	160.4	4.8	1.1
06 04 26.6	-5 57 50	15.2	14.5	13.9	0.6	0.2	74.2	6.2	3.1
06 03 51.3	-5 57 47	...	17.6	15.8	5.1	1.0	138.4	4.2	5.2
06 05 09.6	-5 57 46	18.5	17.3	15.9	2.4	0.7	107.4	7.2	2.5
06 04 55.5	-5 57 29	17.9	16.8	16.0	2.6	0.5	175.1	3.9	0.4
06 04 25.3	-5 57 14	18.2	17.0	15.7	3.5	0.6	151.4	3.9	3.5
06 04 15.2	-5 56 56	15.2	14.2	13.4	2.2	0.2	145.6	2.1	2.0
06 05 06.9	-5 56 50	16.7	15.8	14.9	1.4	0.3	20.5	5.2	1.5
06 04 32.6	-5 56 50	16.7	15.9	15.2	0.9	0.3	93.0	9.0	5.9
06 03 58.5	-5 56 24	17.6	16.3	15.1	1.5	0.4	142.3	6.5	3.6
06 04 09.2	-5 56 22	16.2	15.2	14.4	1.3	0.2	125.5	4.3	2.1
06 04 52.7	-5 56 22	16.1	15.1	14.1	0.6	0.2	101.2	7.9	0.4
06 04 12.4	-5 56 21	18.1	17.2	16.4	1.9	0.6	132.6	9.7	1.6
06 04 38.3	-5 56 03	13.9	13.3	12.9	0.6	0.2	51.2	4.9	7.1

'I'AIll .E 1- *Continued*

α (1950) hh mm ss	δ (1950) (I[I mm ss v	R_c	L_c	P %	ΔP %	θ	Δθ	A_v
'060129.5	-55560	17.0	15.4	14.1	1.0	0.2	1'/2 9	5.3	5.0
060136.6	-55543	18.6	17.1	15.7	2.9	0.6	156.2	5,5	8.1
060505.6	-55539	18.4	1"/.3	16.5	3.()	0.8	7.-I	3.3	2.0
060352.3	-55513	.	18.3		5.4	1.8	140.-/	5.6	1.6
060122.5	.554 5X	1s.?	14,4	13.8	1.1	().2	74.5	3.()	2,9
0604 0s.2	-55423	15.9	14,9	14.1	0.6	().2	144.9	9.3	1.8
06 05 15.5	-55406	17.1	16.()	15.2	1,9	0..4	69.()	5.9	1.5
06 05 10,7	-5 5056	15.8	14.9	13.3	1.1	().3	129.0	5."1	0.5
060109.2	.55046	14.7	14.0	12.5	2.4	().3	150s	4.3	2.2
0605 17.6	-55029	16.1	15.6	13.9	1,9	0.4	101.-/	3.6	2.8
0601316	-55009	16.3	15.5	13.9	1.5	0.4	157.2	8.0	4.8
0601 44.1	-54953	16.4	15.9	14.6	1.5	().s	101.3	6.6	2.3
0605025	.5 4908	13.1	13.2	12.3	0.6	0.2	99.4	7.1	1.0
060522.1	-548 38		15.7	13.9	1.6	0.4	1"/"/.9	6.4	0.7
060120.0	-548 05	15.1	14.6	13.3	2.2	0.3	144.2	5.(I	2.9
06 05 09.6	-54759	13.5	13.5	12.6	0.9	0.2	89.4	5.8	0.5
0601 16.3	-54756	16.4	15.8	14.4	2.1	0.4	142.5	3,9	2.6
060123.5	-54755	16.3	15.0	13,0	3.1	0.4	148.6	3.5	3.3
060138.4	.54743	15.6	15.5	14.4	I.4	0.4	S1.2	4.2	3.6
060122.7	-54735	13.9	13.9	12.9	1.3	0.3	78.5	4.3	3,4
060120.2	-54707	15.9	15.6	14.3	1.5	0.4	140.3	4.4	3.1
060131.2	-546 58	16.1	15.8	14.6	1.5	().4	165.3	6.4	3.1
0601 14.7	-54.559	13,6	13.1	11.6	1.2	().2	143.9	9.4	0.9
060125.2	-54545	14.8	14.8	13.8	0.9	0.3	104.4	6."1	1.9
060133.6	.54543	13.4	13,5	12.6	0.9	[).2	81.5	3.3	3.5
06 04 16.6	-545 ()()	13.8	13.9	13.0	0.9	().3	96.2	4,2	1.3
060119,4	-54456	16.8	16.2	14.8	3.1	0.6	174.1	4.4	1,9
060526.2	-54357	14.0	14.0	13.0	1.0	0.2	75.()	3,7	1.1
060526.0	-541 16	15.7	15.4	14.2	2.0	0.3	29.6	1.9	0.5
060407.8	-54055	15.4	13.4	.	I.7	0.3	107,3	4,2	1.5
0601001	-54014	15.3	15.1	13.9	1.0	().3	115.1	8.4	2.0
060524.6	.539]7	15.1	15.0	14.0	1.0	0.3	40.1	7.5	0.4
0601 13.5	-53915	14.8	14.6	13.4	1.0	0.3	141.0	6.4	1.8
06 0405.1	-5 38 50	12.8	13.0	12.1	0.9	0.2	66.6	15,2	1.4
060122.3	-53823	14.1	13.7	123	1.2	0.2	146.5	3.3	2.1
0601 22.9	.53806	14.2	14.3	13.3	I.3	0.3	146. I	5.2	2.2
06 04 11,2	-53741	14.?	13.5	11.9	1.(1	(),2	130.6	6.9	2.s
06 0411.1	-53647	16.8	16.5	15.2	21	().-/	157.6	x.7	1.8
060135.3	-53540	16.4	15.9	14.3	1.8	().6	135.0	8.8	4.7
060107.2.	-53537	14.9	14.8	13.8	1.0	().3	154.1	8.8	0.8
0604 29.9	-53534	16.9	16.2	14.6	3.5	0.6	146.3	2,2	2.6
06 OS 23.9	-53453	13.6	13.6	12.8	0.9	0.2	76.0	4.1	4,7
06 04 33.2	-533 2(I	17.()	16.7	15.4	3.6	().8	147.3	5.2	2.9
0601 19.3	-s 33 10	17.0	16.5	15.2	2.x	0.9	143.)	8.4	1.1
060131.8	-53233		16.5	]5.3	2.7	0.8	11S.7	(), s	2.7
06 0404.3	-53155	...	17.9	16.7	8.5	2.8	130.7	13,6	1.2
060142,8	-531 10	13.9	13.8	12.9	0.7	0.2	66.4	5,2	2.6
0601 2S.7	-.53012	14.4	14.3	13.3	1.1	0.3	90.9	5.1	0.8
0605 OS.7	-52947		14.8	12.3	3.1	().3	154.1	2.()	2.9
060524.6	.52938	15.0	14.7	13.4	2.1	0,3	40.4	3.6	6.2
060503.6	-52904	14.2	13.6	12.1	0.9	0.3	96.9	4.0	3.0

Table Notes: The coordinate positions are accurate to 10 - 1 5 " . The estimated photometric errors **of the** (V, R, 1) photometry is -1 0%. The degree of' polarization, P, and its uncertainty, Al', are expressed as percentages. The angle of polarization, O, and its uncertainty, AO, are expressed in degrees counterclockwise from position angle ()'' (north). The visual extinction, A_v, is estimated from the molecular gas column density of Mon R2.

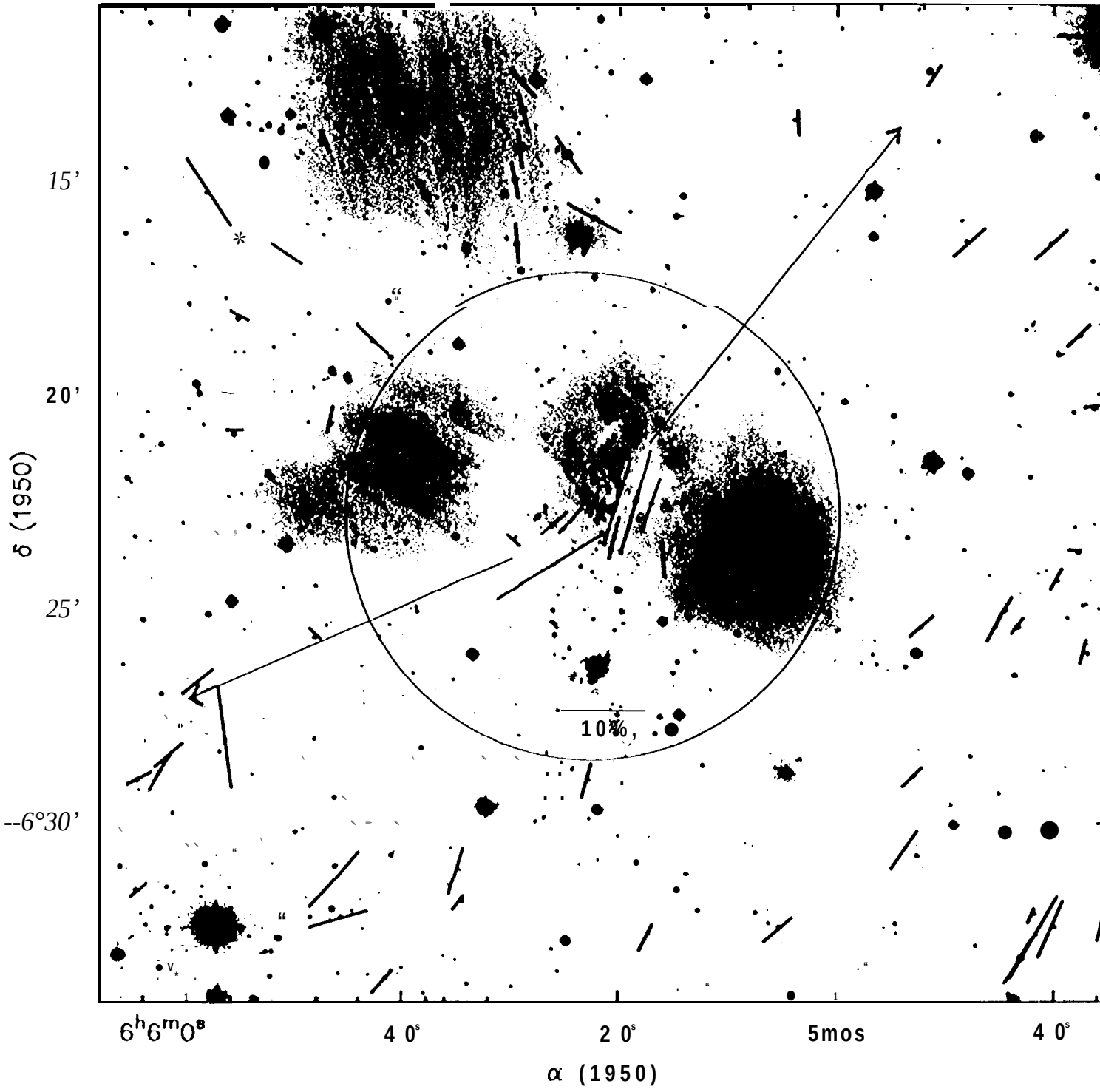

Figure 1

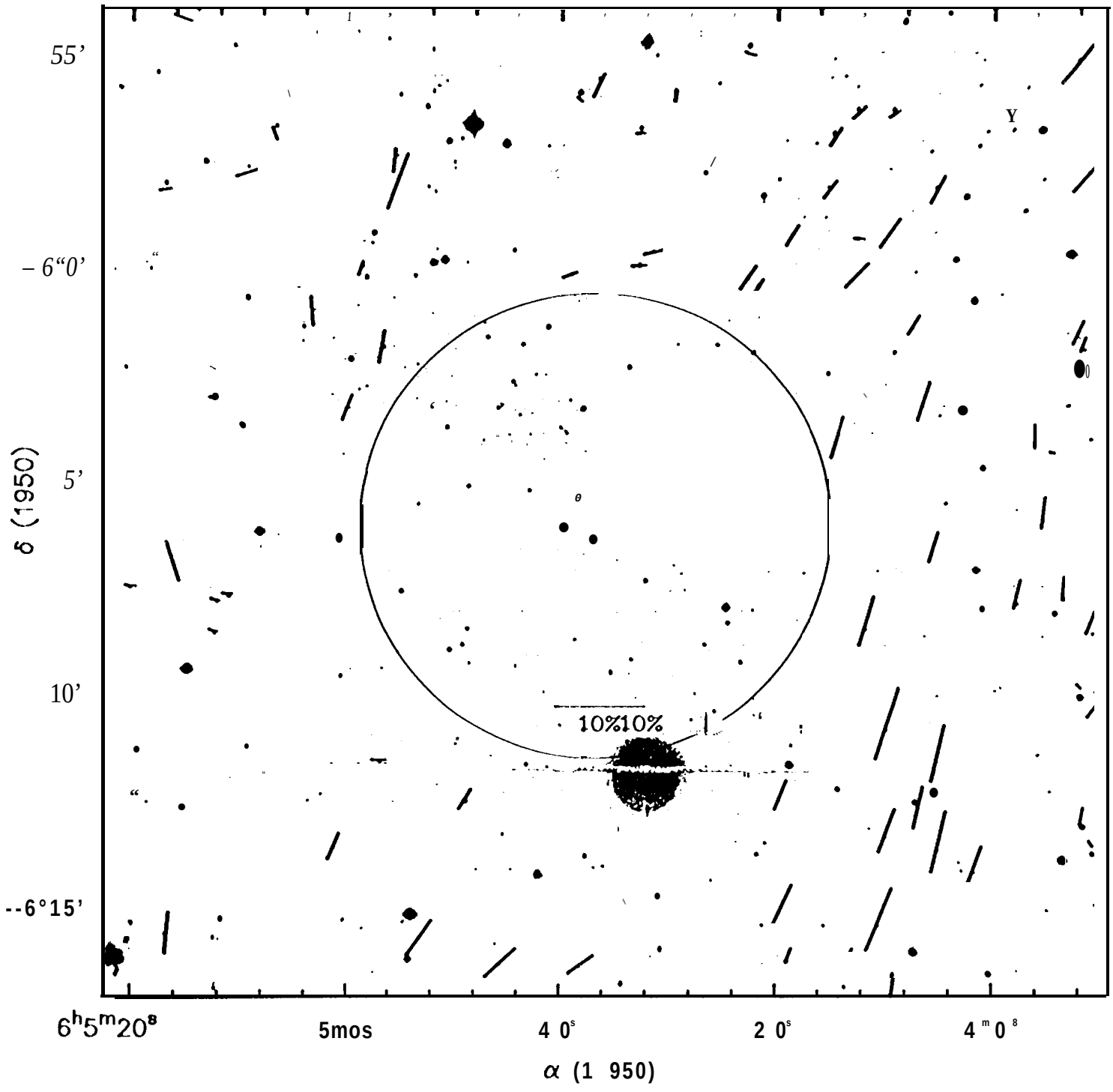

Figure 2-

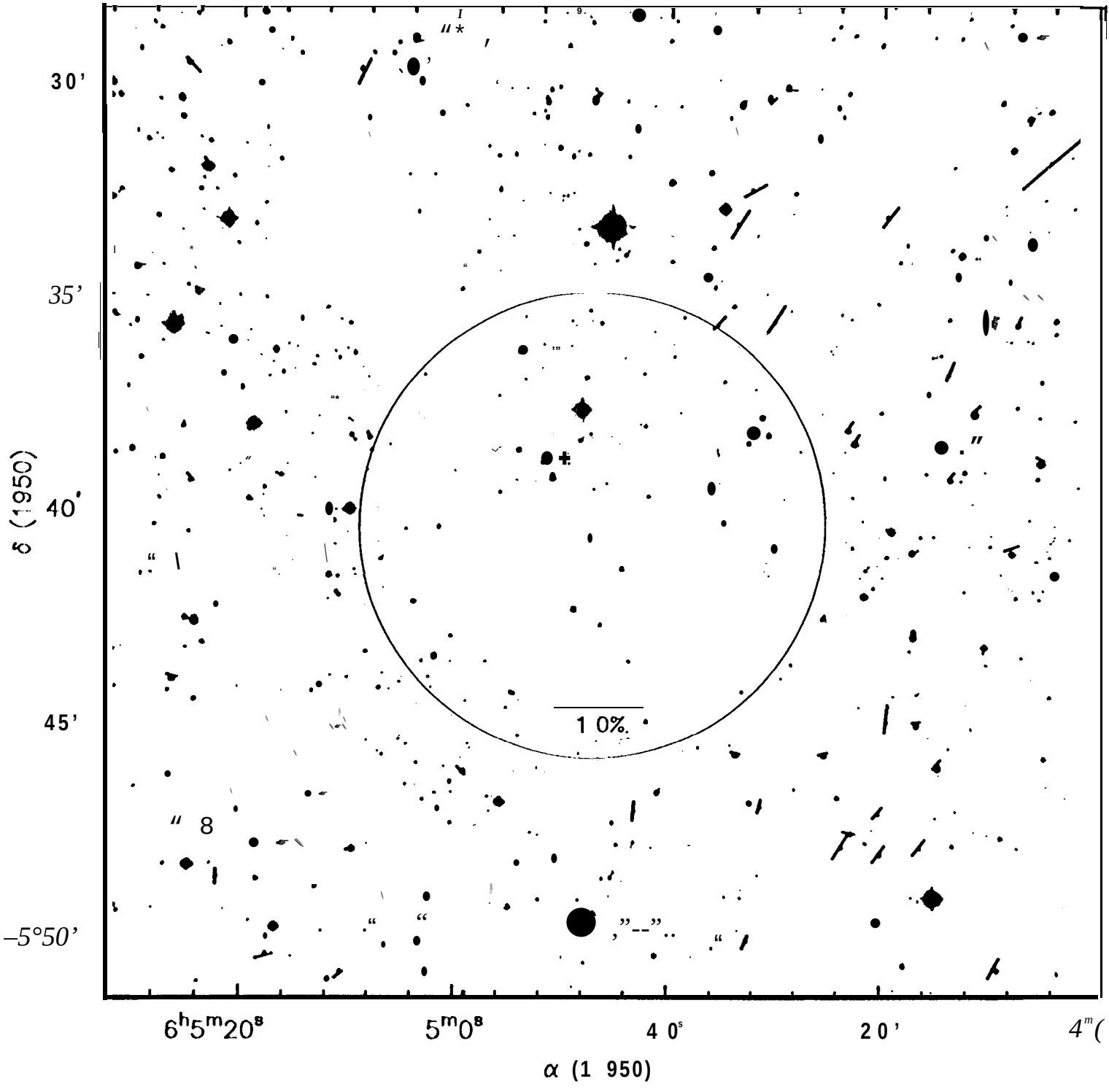

Fig. 3

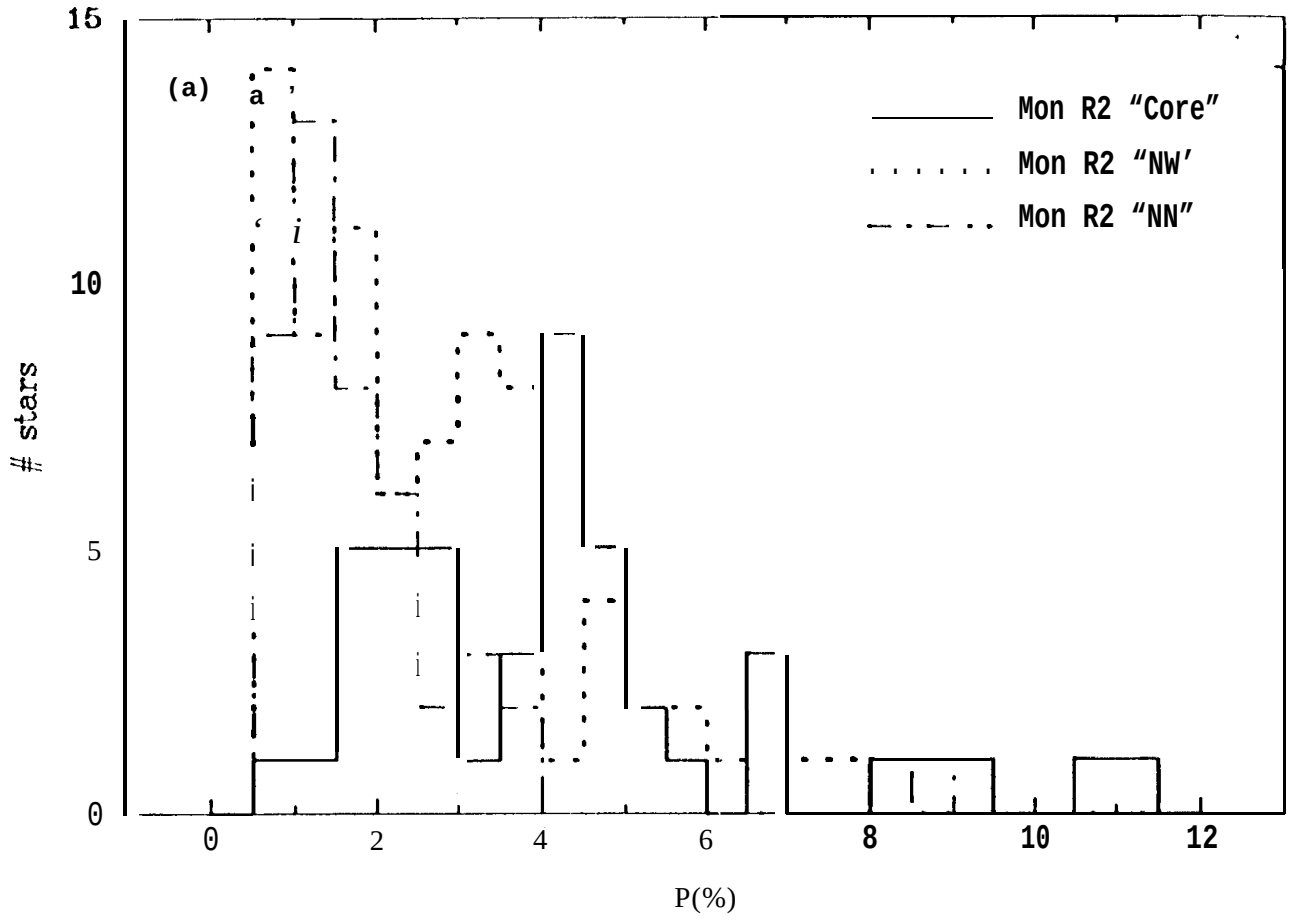

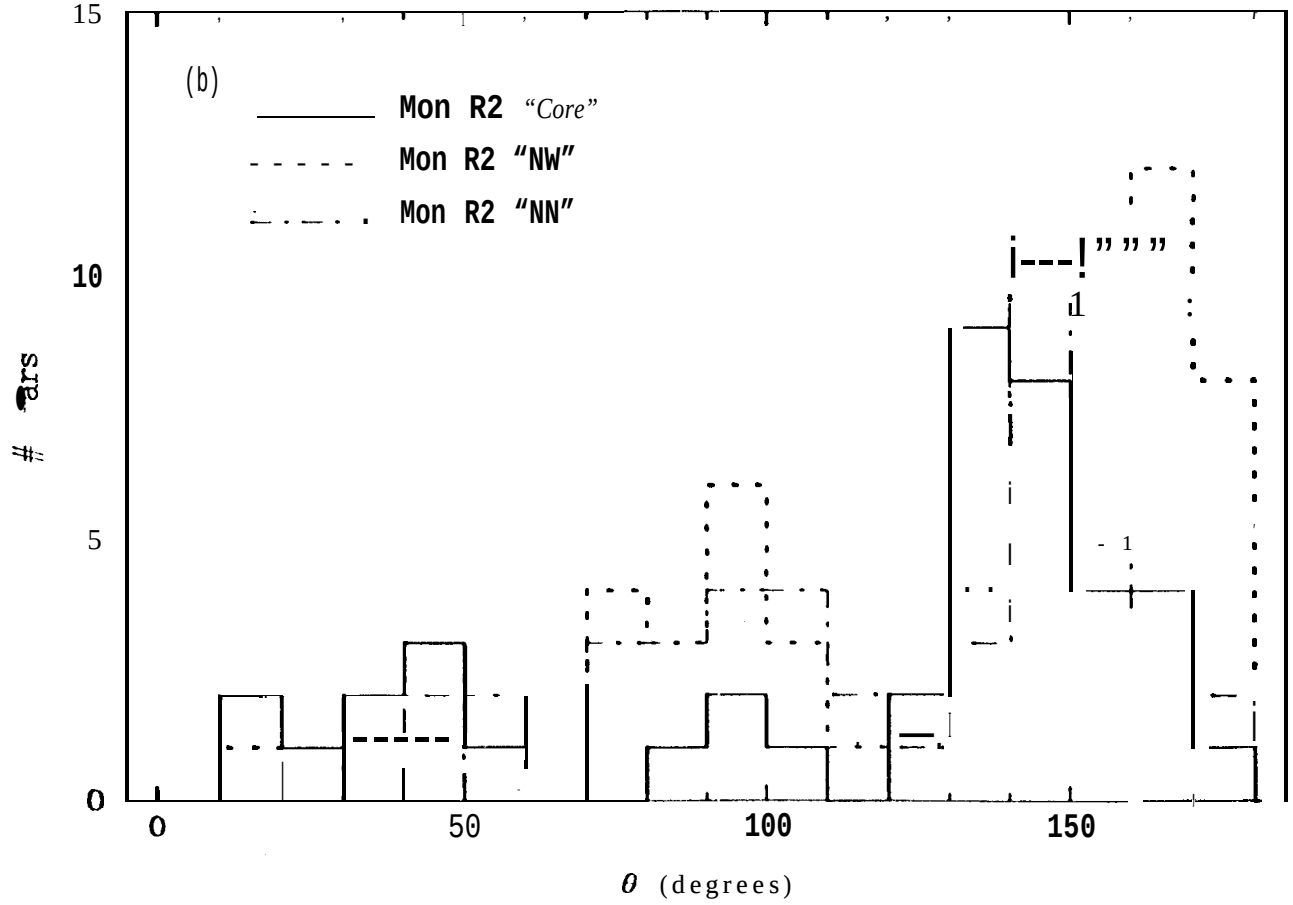

Figure 4
Jarrett et al.

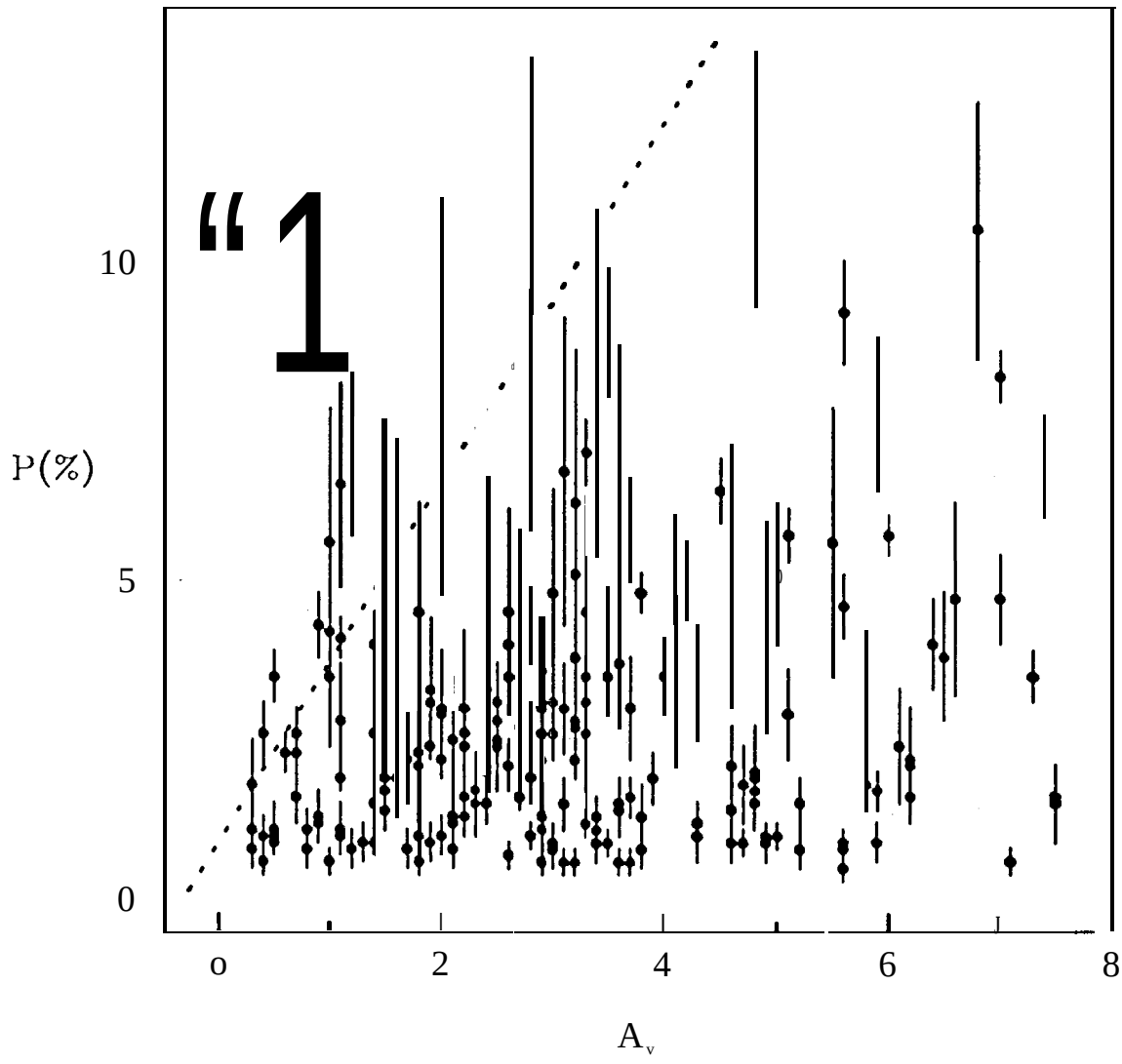

Figure 5

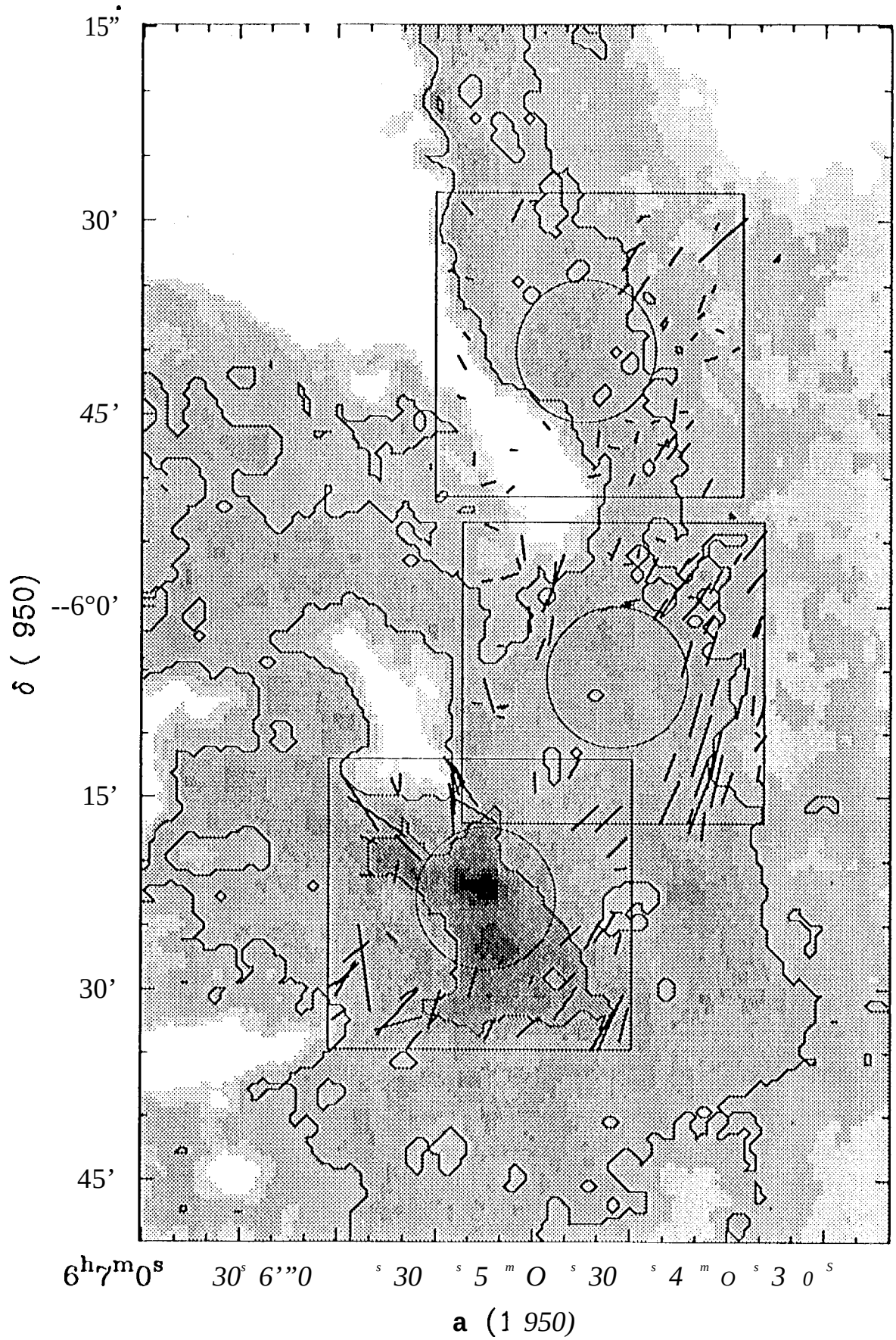

Figure 6 Jarrett et. al.